

Geometric Sampling Framework for Exploring Molecular Walker Energetics and Dynamics

Bruna Jacobson
Department of Computer Science
University of New Mexico
Albuquerque, New Mexico 87131-0001
bjacobson@unm.edu

Jon Christian L. David
Department of Computer Science
University of New Mexico
Albuquerque, New Mexico 87131-0001
jdavid@cs.unm.edu

Mitchell C. Malone
Department of Computer Science
University of New Mexico
Albuquerque, New Mexico 87131-0001
mmalone1@unm.edu

Kasra Manavi
Department of Computer Science
University of New Mexico
Albuquerque, New Mexico 87131-0001
kazaz@cs.unm.edu

Susan R. Atlas
Department of Physics and
Astronomy
Department of Computer Science
University of New Mexico
Albuquerque, New Mexico 87131-0001
susie@sapphire.phys.unm.edu

Lydia Tapia
Department of Computer Science
University of New Mexico
Albuquerque, New Mexico 87131-0001
tapia@cs.unm.edu

ABSTRACT

The motor protein kinesin is a remarkable natural nanobot that moves cellular cargo by taking 8 nm steps along a microtubule molecular highway. Understanding kinesin's mechanism of operation continues to present considerable modeling challenges, primarily due to the millisecond timescale of its motion, which prohibits fully atomistic simulations. Here we describe the first phase of a physics-based approach that combines energetic information from all-atom modeling with a robotic framework to enable kinetic access to longer simulation timescales. Starting from experimental PDB structures, we have designed a computational model of the combined kinesin-microtubule system represented by the isosurface of an all-atom model. We use motion planning techniques originally developed for robotics to generate candidate conformations of the kinesin head with respect to the microtubule, considering all six degrees of freedom of the molecular walker's catalytic domain. This efficient sampling technique, combined with all-atom energy calculations of the kinesin-microtubule system, allows us to explore the configuration space in the vicinity of the kinesin binding site on the microtubule. We report initial results characterizing the energy landscape of the kinesin-microtubule system, setting the stage for an efficient, graph-based exploration of kinesin preferential binding and dynamics on the microtubule, including interactions with obstacles.

KEYWORDS

Molecular walkers; kinesin; motion planning; OBPRM; energy landscape; protein-protein interaction; motor protein

ACM acknowledges that this contribution was authored or co-authored by an employee, or contractor of the national government. As such, the Government retains a nonexclusive, royalty-free right to publish or reproduce this article, or to allow others to do so, for Government purposes only. Permission to make digital or hard copies for personal or classroom use is granted. Copies must bear this notice and the full citation on the first page. Copyrights for components of this work owned by others than ACM must be honored. To copy otherwise, distribute, republish, or post, requires prior specific permission and/or a fee. Request permissions from permissions@acm.org.
ACM-BCB'17, August 20-23, 2017, Boston, MA, USA.
© 2017 ACM. 978-1-4503-4722-8/17/08...\$15.00
DOI: <http://dx.doi.org/10.1145/3107411.3107503>

1 INTRODUCTION

The motor protein kinesin-1 (henceforth referred to as kinesin) is a molecular walker responsible for intracellular cargo transport. The full protein structure contains two catalytic domains (heads) responsible for procession; a neck linker that connects the heads to its stalk; and a long coiled-coil structure that binds to the cargo. The protein walks on microtubule tracks [25, 28]. Microtubules are composed of 13 protofilament chains of α and β tubulin heterodimer subunits (see Figure 1a). Normally kinesins walk along a single protofilament on microtubules, however sidestepping is known to occur under certain conditions [12].

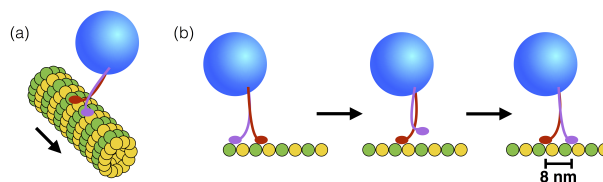


Figure 1: (a) Illustration of kinesin walking along a microtubule comprised of 13 protofilaments. Green and yellow disks represent α and β tubulin heterodimers. Kinesin is shown in red and purple. The blue bead attached to the stalk represents the cargo. (b) Hand-over-hand kinesin walk. The catalytic domains or heads (red and purple) bind to the microtubule and alternate leading position during the walk, in a hand-over-hand fashion.

A kinesin catalytic head consumes one ATP molecule to take each 8-nm hand-over-hand step in one-dimensional transport along the microtubule [30], Figure 1b. There is currently a large body of experimental and theoretical work on the biophysical, biochemical, and dynamical properties of kinesin. However, the molecular details of how kinesin transforms the chemical energy from ATP hydrolysis into a mechanical step are not yet fully understood.

The interaction of the kinesin catalytic heads with the microtubule as it walks can be characterized as protein binding and

unbinding events. During each step the kinesin catalytic head binds to a microtubule subunit, the α - β tubulin heterodimer. Binding sites on the microtubule correspond to low energy configurations of the microtubule-kinesin complex.

The goal of the present work is to develop a model of the kinesin-tubulin interaction energy landscape to enable full dynamical simulations. We utilize the Probabilistic Roadmap Method (PRM) [15], a method originally developed for identifying robotic motions. Specifically, we apply the PRM variant, Obstacle-based Probabilistic Roadmap Method (OBPRM) [3], that samples configurations on surfaces prior to connecting nearby configurations with weighted edges. The resulting roadmap enables the study of kinesin interactions with the microtubule surface through the sampling of potential binding sites and possible trajectories. The roadmap is generated by creating a three-dimensional model of the kinesin head and microtubule system based on their protein crystal structures, and efficiently sampling the conformational space of the interacting molecules. For each sampled conformation, we compute the all-atom energy of the interacting system to determine the energy landscape explored by the kinesin head as it executes diffusive motion before binding to the microtubule.

2 RELATED WORK

The energy landscape around the microtubule has been investigated in the context of the kinesin walk via several physics-based methods. In [11], the authors used Brownian dynamics coupled with a Poisson-Boltzmann approach to study the electrostatics-induced bias of the kinesin head search to the binding site on the microtubule. Their method did not include van der Waals energy terms, which are important when the two molecules are in close proximity. A multiscale Poisson-Boltzmann method was applied in [16] to compute the electrostatic interaction between kinesin and the microtubule. In this work, the authors included a van der Waals energy term, but the Poisson-Boltzmann electrostatics component used precomputed regular grids with fine sampling only in the vicinity of assumed binding sites, causing potential loss of ruggedness detail elsewhere on the microtubule surface.

Simulation and modeling of macromolecular interactions have been extensively discussed in [17]. A comprehensive review of robotics-inspired methods for protein folding is given in [21]. Motion planning algorithms have been extensively applied to molecular simulations [2, 19], including protein folding pathways [22, 23, 27]. In particular, simulation of receptor-ligand binding has been carried out using OBPRMs [3, 4]. These techniques have been shown to be successful at capturing kinetic information for RNA [26] and proteins [27].

3 METHODS

3.1 Models

The starting models for kinesin and tubulin were obtained from the Protein Data Bank. We used the kinesin/microtubule structure from PDB ID 4LNU. This structure represents one kinesin head bound to a tubulin heterodimer [8]. Additional chains, nucleotides, other ligands, and water in the original 4LNU structure were removed using Pymol [10]. The resulting structure has 3 chains: A, B, and

K, representing α -tubulin, β -tubulin, and the kinesin head, respectively. The head is composed of 309 amino acids and 4,824 atoms, and the α - β tubulin heterodimer has 870 amino acids and 13,464 atoms. The final structure is shown in Figure 2.

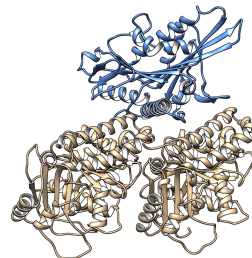


Figure 2: Protein structure from the Protein Data Bank used in this work, PDB ID 4LNU. Additional chains, nucleotides, ligands and water have been removed. The kinesin head is shown in blue and the microtubule heterodimer in tan.

To construct the microtubule patch, we used a 3D electron microscopy (EM) map from [24], and the crystal structure of the tubulin heterodimer for the microtubule subunits. Several copies of 4LNU were fit to the EM map using the rigid fit feature in Chimera [20]. We then created a 3-by-3 patch of heterodimers (9 total) to model the microtubule surface. The patch is comprised of 7,830 amino acids and 121,176 atoms. In the cleaned model of 4LNU, the α - β tubulin heterodimer is aligned to the central heterodimer in the 3-by-3 patch, placing the kinesin head into a bound state relative to the microtubule model, shown in Figure 3.

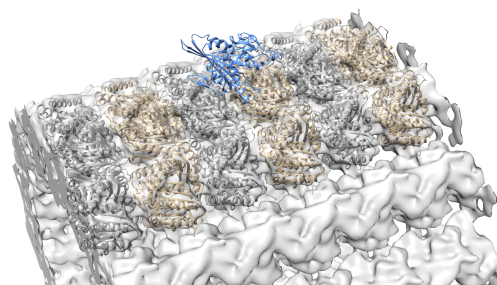


Figure 3: Fitting PDB structure of microtubule heterodimer and kinesin head to EM map of microtubule.

Once the microtubule patch has been created, as a single structure with a kinesin bound to the middle of the patch, hydrogens were added via Chimera (Figure 4, left). Then the kinesin and microtubule patch structures were separated into two PDB files. To apply OBPRM to the molecules, it is necessary to generate three-dimensional geometric structure models that capture protein surface ruggedness. Geometric models were created for the kinesin and patch structures via the *Multiscale Models* option in Chimera to make models (with parameter resolution set to 8), with results as shown in Figure 4 (right).

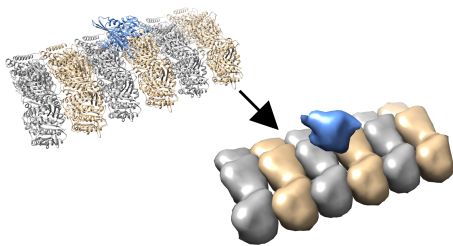


Figure 4: Left: Microtubule patch with a bound kinesin head resulting from EM fit. Right: Geometric model obtained by generating a 3D model of the protein structure.

The geometric centers of mass of the models of the kinesin head and the microtubule patch were found using the IVCON package [7]. These values were recorded and the 3D modeling tool Blender [5] was used to center them. Centering is done by translating the two models (of kinesin head and microtubule patch) such that both geometric centers of mass are set to the origin of the coordinate system. If x_{iv} , y_{iv} , and z_{iv} are the geometric centers of mass as reported by IVCON, then the translation vector used in Blender is: $x = -x_{iv}$, $y = z_{iv}$, and $z = -y_{iv}$, since IVCON and Blender use different coordinate systems. It is important to note that the geometric center of mass of the geometric model is not the same as the center of mass of the PDB structure. All calculations were performed with respect to the geometric center of mass.

3.2 Generating Configurations with OBPRM

We use OBPRM to create configuration samples of the kinesin head. Before sampling begins, we restrict configuration generation to a sampling region on the microtubule surface with dimensions $x \in [-70, 75]$, $y \in [-20, 150]$, and $z \in [-125, 125]$ Å. The three dimensions correspond to longitudinal length (around the microtubule curvature, x), vertical distance from the microtubule (height, y), and length parallel to the microtubule long axis (z). Two initial configurations are chosen randomly within this sampling region, such that one configuration is in collision with the microtubule and the other configuration is not. By connecting the two configurations' geometric centers we create a vector that points outwards in a random direction.

Binary search is performed along this vector to find the configuration of the kinesin head where the microtubule and kinesin head surfaces are within a given positional resolution but not in collision. This configuration and the vector are used in order to guide the creation of new samples at 5 Å intervals along the vector. We take one kinesin head sample towards the minus end of the vector (into the microtubule), and four samples toward the plus end of the vector (outside the microtubule). For each of these samples we perform a random rotation of the kinesin head with respect to its native bound position, for which the pitch (α), yaw (β), and roll (γ) angular values are all restricted to $[-5^\circ, 5^\circ]$. The procedure is repeated until 100,000 configurations have been generated. The positions of the center of mass of the resulting samples are illustrated in Figure 5. It should be noted that retention of the configuration along the vector toward the microtubule surface is not standard

in OBPRM, and may produce configurations in collision, which have high energy. We chose to generate and retain these samples because it is important to identify binding configurations, possibly in tight proximity to the microtubule surface. Since each sample is subsequently evaluated energetically, possible high-energy samples can be easily identified and disregarded when low energy paths are followed.

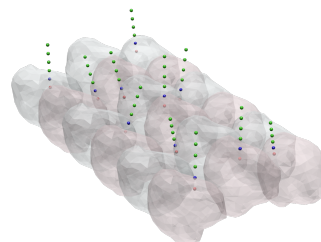


Figure 5: Illustration of OBPRM sampling of kinesin head. Example configurations are samples along vectors as shown, at 5 Å intervals. Green dots: Position of the center of mass of the kinesin head, which is treated as a rigid body. Blue dots: Samples on the surface of the microtubule. Red dots: Samples within the microtubule. The direction of the line is chosen randomly. Rotations are randomly chosen within $[-5^\circ, 5^\circ]$ for all three rotational degrees of freedom.

3.3 Energy calculations

Once all configurations of the kinesin head and the microtubule have been generated, we compute the interaction energies between the two molecules at each configuration. We use our in-house software *Molecular Docking Game* (MDG) to move the kinesin head to each configuration [1]. Both the kinesin head and microtubule patch are kept rigid.

The interaction energy is given by the sum of the electrostatic energy and the van der Waals energy, as represented by the non-bonded energy terms in molecular dynamics force fields [6, 29]. The terms are computed for intermolecular interactions only.

The electrostatic energy between atom i in the kinesin head and atom j in the microtubule, U_{ij} , is:

$$U_{ij} = \frac{q_i q_j}{4\pi\epsilon_0 r_{ij}}, \quad (1)$$

where $q_{i(j)}$ is the charge of atom $i(j)$, and r_{ij} is the distance between the atoms. The van der Waals interaction between atom i in the kinesin head and atom j in the microtubule, V_{ij} , is:

$$V_{ij} = \epsilon_{ij} \left[\left(\frac{\sigma_{ij}}{r_{ij}} \right)^{12} - 2 \left(\frac{\sigma_{ij}}{r_{ij}} \right)^6 \right], \quad (2)$$

where the parameter ϵ_{ij} is the depth of the potential well, and σ_{ij} is the distance at which the potential between the atoms vanishes. The total energy for the system is:

$$E = \sum_{i=1}^K \sum_{j=1}^M (U_{ij} + V_{ij}), \quad (3)$$

where the sum over i runs over all K atoms in the kinesin head, and the sum over j is over all M atoms in the microtubule.

MDG uses the Amber94 [29] force field parameters to compute energies. These energies are calculated for atoms out to a maximum distance of 12 Å. The electrostatic and van der Waals energies have discontinuities at the 12 Å cutoff, going to zero for intermolecular atomic pairs whose distance is greater than 12 Å.

3.4 Roadmap Connectivity

We construct a graph such that each node i is connected to all nodes j whose distance between i and j is less than or equal to $k = 5$ Å. All edges are bidirectional. The edge weight W_{ij} is defined as the energy difference between the nodes:

$$W_{ij} = E_j - E_i. \quad (4)$$

The connected component of this roadmap includes the kinesin bound state. To simulate how kinesin navigates the energy landscape on the microtubule by finding low energy paths to the bound state, we use Dijkstra’s algorithm to find the lowest weighted path to the known native state, where the initial and final states are defined for each run.

4 RESULTS

We used OBPRM from the Parasol Motion Planning Library from Texas A&M University to generate the 100,000 configurations in parallel on a Dell PowerEdge R620 with an Intel Xeon E5-2670, 2.6 GHz processor. This machine has 24 nodes, 16 cores per node, 4GB of RAM per core, and runs Scientific Linux OS.

Both the kinesin head and the microtubule are treated as rigid bodies. The microtubule is held fixed, and the six degrees of freedom of the center of mass of the kinesin head, three spatial and three rotations, are stored for each configuration. For the points that are not in collision, the node density is nearly 0.32 nodes/Å³, which results in an average shortest distance between nodes of about 0.9 Å. In the connected roadmap there are 99,999 nodes and 6,375,848 total edges, with on average 127.5 edges per node.

MDG is used for the energy calculations. The 6-dimensional degrees of freedom of the configurations, and the atomic positions (PDB files) of all molecules are used as input. A supercomputer cluster with 24 nodes, 16 cores per node, and 4GB of RAM per core was used to compute the energies, to sample kinesin positions and to connect nodes in the roadmap.

Timing results for sampling, energy, and connectivity calculations are shown in Table 1.

Table 1: Timing Results for Sampling, Energy, and Connectivity Calculations.

	Sampling	Energy	Connectivity
CPU-time (s)	3.191×10^2	1.304×10^7	2.083×10^2

By construction, some configurations are generated in collision with the microtubule (Figure 6). The distribution of energies found with the MDG that are lower than 2000 kcal/mol is shown in Figure 7. A few energy values, as high as 10^{28} kcal/mol, were found;

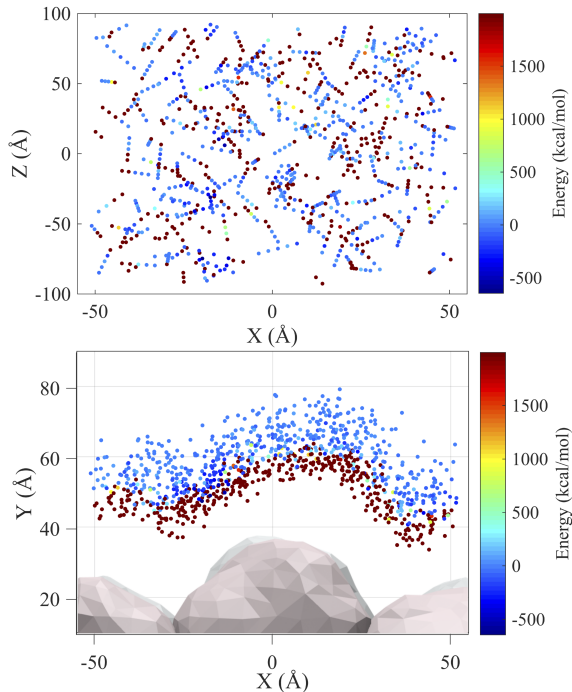


Figure 6: First 1000 configurations generated using the methodology described in the text. Top: Two-dimensional xz (top) view of the microtubule surface. The kinesin head is sampled by moving its center of mass 5 Å along lines started at random positions on the microtubule. The transition from collision to non-collision states is identified by the configuration energy value, as the points on a line move from high energies (red) to low energies (blue). Bottom: Same data shown in xy plane.

however these correspond to unphysical configurations in collision. In Figure 8, we show the distribution of positive and negative energy values along the length of the microtubule patch. The periodic peaks on the histograms are out of phase by about $\pi/2$, showing an increase in positive energies (possibly related to collision) when there is a decrease in negative energies. Peaks in negative energies occur at ≈ 40 Å intervals in the z axis, coinciding with the region where the α and β tubulins are joined along a single protofilament.

This periodic effect for low energy regions is also seen in the energy plot on the xz plane, Figure 9. Here we see a concentration of low energy values (< -500 kcal/mol) at the intersection of α and β tubulins along a protofilament.

We also observe that some low energy clusters are broader than others. The clusters where binding positions exist (near $-80, 0,$ and 80 Å in the z axis) are narrower than clusters where binding of kinesin to the microtubule does not occur (near $z = -40$ Å and $z = 40$ Å).

To understand how the low energy regions influence kinesin stepping, we examined whether lowest weighted Dijkstra pathways connecting random nodes choose to visit these regions. We analyzed two lowest-weighted Dijkstra paths in this energy landscape. The

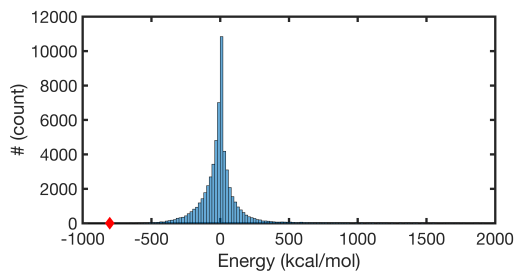


Figure 7: Energy distribution histogram for kinesin and microtubule system. Only energy values less than 2000 kcal/mol are shown, but a few high energy values (as high as 10^{28} kcal/mol) also appear for collisions. The bound state energy is shown as the red diamond at $E_{bound} = -803.35$ kcal/mol. The location of the peak at zero energy is due to the large number of configurations for which all kinesin and microtubule atoms are separated by a distance greater than 12 Å.

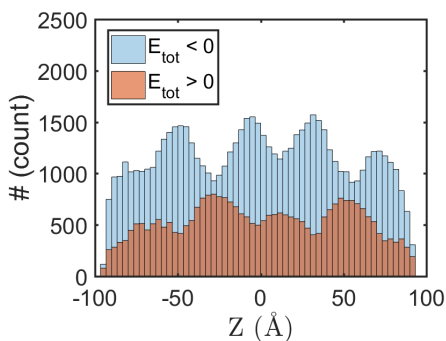


Figure 8: Histogram of positive (red) and negative (blue) energies along the microtubule axis. There are more negative energy values overall, but peaks in negative energies correspond to troughs in positive energy and vice-versa, with ≈ 40 Å spacing. High positive energy values are due to collisions between the kinesin head and the microtubule.

first connects a random initial state with zero energy (the black \circ in Figure 10) to the first microtubule bound state (positioned at the black \times in Figure 10). The second Dijkstra pathway starts from this bound state and ends at a second bound state about 80 Å away, toward the minus z axis (the black \triangleleft in Figure 10).

As shown in Figure 10, the Dijkstra pathway tends to stay along a single protofilament and visits every low energy region on the protofilament between the start and end states. The path takes the kinesin head away from the microtubule surface in between these regions when passing through a high energy barrier.

5 DISCUSSION AND CONCLUSIONS

We have shown that motion planning methods allied to a physics-based model are successful in locating the low energy configurations in the interaction energy landscape of two macromolecules.

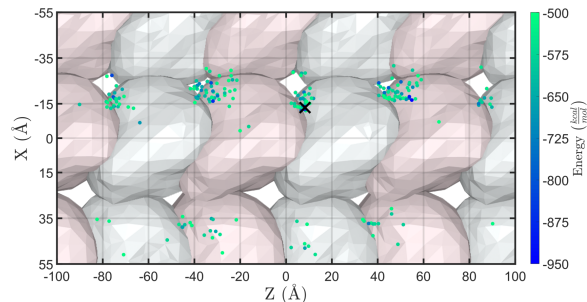


Figure 9: Low energy configurations on the microtubule surface. Each point corresponds to the position of the center of mass of the kinesin head. The black \times at $x = -13.33$ Å, $z = 8.28$ Å corresponds to the position of the center of mass of the native bound state of the kinesin head. Note the periodic pattern of the location of low energy valleys, at approximately every 40 Å along the protofilament.

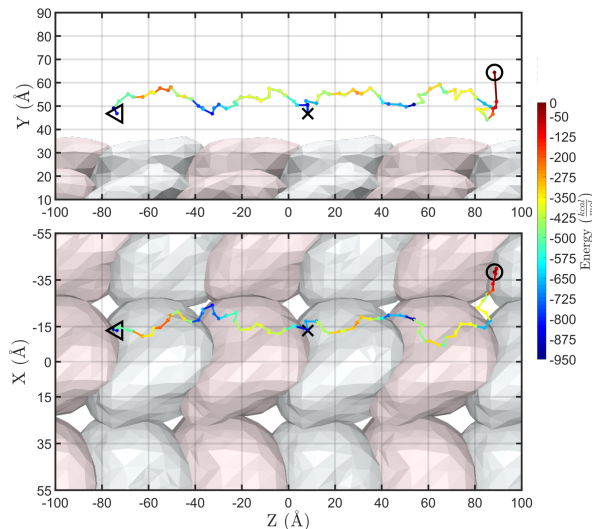


Figure 10: Two-dimensional yz (top) and xz (bottom) views of two Dijkstra runs showing lowest-weighted paths from $x = -38.31$ Å, $y = 64.33$ Å, $z = 88.44$ Å (shown as a black \circ), to a kinesin-microtubule bound state at $x = -13.33$ Å, $y = 46.76$ Å, $z = 8.28$ Å (shown as a black \times), and from this bound state (\times) to a second bound state at $x = -13.33$ Å, $y = 46.76$ Å, $z = -73.52$ Å (shown as a black \triangleleft). At the initial point, the kinesin head is far from the microtubule and the interaction energy is zero. Note that both paths visit all low energy regions along the same protofilament between the start and goal (see Figure 9 for location of low energy basins).

These locations are associated with targets for protein-protein binding. Our simulations corroborate experimental evidence that a kinesin head without nucleotides (ATP or ADP) has strong interactions with binding sites on the microtubule [9]. These strong interaction regions, the low energy basins, appear at the native binding sites, but also exist in between binding sites, showing a

periodic pattern at approximately every 40 Å along each protofilament. Since the kinesin step is 8 nm in length, the appearance of these low energy states in between step locations supports the possibility of a substep. Such 4-nm substeps have been proposed in models [13] but so far they have eluded experimental detection, due to the need to observe fast time scales at high spatial resolution. However, more recent experiments have been approaching this limit, and previously undetected states of the protein during its walk have now been observed [14, 18]. Our lowest weighted Dijkstra pathways demonstrated a low energy pathway along a single protofilament. This reflects experimentally observed behavior that finds progression along a single protofilament instead of sidestepping [25]. In addition, all low energy regions along the protofilament are visited, further indicating that these low energy regions may indeed correspond to substeps. To investigate this possibility, we plan to perform a kinetic analysis to compute lifetimes of the kinesin head at the intermediate low energy regions, with longer lifetimes suggestive of metastable substep positions. The application of motion planning methods for the kinesin walk may prove particularly important when considering that the microtubule is in reality decorated with stabilizing proteins (such as tau protein), and crowded with other molecular walkers. For these situations, motion planning will enable studies of how kinesin avoids colliding with these obstacles and continues its walk by switching to an adjacent protofilament.

6 ACKNOWLEDGEMENTS

The authors are thankful to Torin Adamson for his assistance in setting up and running some of the computational models. We also thank the Center for Advanced Research Computing (CARC) at UNM for providing computational resources and support. This work is supported by the National Science Foundation (NSF) (S.R.A.) and under NSF Grant Nos. CCF-1518861, IIS-1528047, IIS-1553266 (L.T., CAREER) and National Institutes of Health Grant P50GM085273 to the New Mexico SpatioTemporal Modeling Center. Any opinion, findings, and conclusions or recommendations expressed in this material are those of the authors and do not necessarily reflect the views of the National Science Foundation.

REFERENCES

- [1] Torin Adamson, John Baxter, Kasra Manavi, April Suknot, Bruna Jacobson, Patrick Gage Kelley, and Lydia Tapia. 2014. Molecular Tetris: Crowdsourcing Molecular Docking Using Path-Planning and Haptic Devices. In *Proceedings of the Seventh International Conference on Motion in Games (MIG '14)*. ACM, New York, NY, USA, 133–138. DOI: <https://doi.org/10.1145/2668084.2668086>
- [2] Ibrahim Al-Bluwi, Thierry Siméon, and Juan Cortés. 2012. Motion planning algorithms for molecular simulations: A survey. *Computer Science Review* 6, 4 (2012), 125–143.
- [3] Nancy M. Amato, O. Burchan Bayazit, Lucia K. Dale, Christopher Jones, and Daniel Vallejo. 1998. OBPRM: An Obstacle-Based PRM for 3D Workspaces. In *Proc. Int. Wkshp. on Alg. Found. of Rob. (WAFR)*. 155–168.
- [4] O. Burchan Bayazit, Guang Song, and Nancy M. Amato. 2001. Ligand Binding with OBPRM and User Input. In *IEEE Int. Conf. on Rob. and Auto.* 954–959.
- [5] Blender Online Community. 2017. *Blender - a 3D modelling and rendering package*. Blender Foundation, Blender Institute, Amsterdam. <http://www.blender.org>
- [6] Bernard R. Brooks, Robert E. Brucoleri, Barry D. Olafson, David J. States, S. Swaminathan, and Martin Karplus. 1983. CHARMM: A program for macromolecular energy, minimization, and dynamics calculations. *Journal of Computational Chemistry* 4, 2 (1983), 187–217.
- [7] John Burkardt, John F Flanagan, Zik Saleeba, Martin van Velsen, Gert van der Spoel, Philippe Guglielmetti, and Tomasz Lis. 2014. *IVCon - a 3D graphics file converter package*. <http://ivcon-tl.sourceforge.net/>
- [8] Luyan Cao, Weiyi Wang, Qiyang Jiang, Chunguang Wang, Marcel Knossow, and Benoît Gigant. 2014. The structure of apo-kinesin bound to tubulin links the nucleotide cycle to movement. *Nature Comm.* 5 (2014), 1–9.
- [9] R.A. Cross. 2016. Review: Mechanochemistry of the kinesin-1 ATPase. *Biopolymers* 105, 8 (2016), 476–482.
- [10] Warren L. DeLano. 2002. The PyMOL molecular graphics system. (2002).
- [11] Barry J. Grant, Dana M. Gheorghie, Wenjun Zheng, Maria Alonso, Gary Huber, Maciej Dlugosz, J. Andrew McCammon, and Robert A. Cross. 2011. Electrostatically Biased Binding of Kinesin to Microtubules. *PLoS Biol* 9, 11 (2011), e1001207.
- [12] Gregory J. Hoepflich, Andrew R. Thompson, Derrick P. McVicker, William O. Hancock, and Christopher L. Berger. 2014. Kinesin's Neck-Linker Determines Its Ability to Navigate Obstacles on the Microtubule Surface. *Biophysical Journal* 106, 8 (2014), 1691–1700.
- [13] Changbong Hyeon and José N. Onuchic. 2007. Mechanical control of the directional stepping dynamics of the kinesin motor. *Proceedings of the National Academy of Sciences* 104, 44 (2007), 17382–17387.
- [14] Hiroshi Isojima, Ryota Iino, Yamato Niitani, Hiroyuki Noji, and Michio Tomishige. 2016. Direct observation of intermediate states during the stepping motion of kinesin-1. *Nature Chemical Biology* (2016).
- [15] Lydia E. Kavrakli, Petr Švestka, Jean-Claude Latombe, and Mark H. Overmars. 1996. Probabilistic roadmaps for path planning in high-dimensional configuration spaces. *IEEE Trans. Robot. Automat.* 12, 4 (August 1996), 566–580.
- [16] Lin Li, Joshua Alper, and Emil Alexov. 2016. Multiscale method for modeling binding phenomena involving large objects: application to kinesin motor domains motion along microtubules. *Scientific Reports* 6 (2016), 23249.
- [17] Tatiana Maximova, Ryan Moffatt, Buyong Ma, Ruth Nussinov, and Amarda Shehu. 2016. Principles and overview of sampling methods for modeling macromolecular structure and dynamics. *PLoS Comput Biol* 12, 4 (2016), e1004619.
- [18] Keith J. Mickolajczyk, Nathan C. Deffenbaugh, Jaime Ortega Arroyo, Joanna Andrecka, Philipp Kukura, and William O. Hancock. 2015. Kinetics of nucleotide-independent structural transitions in the kinesin-1 hydrolysis cycle. *Proc. Natl. Acad. Sci. (USA)* 112, 52 (2015), E7186–E7193.
- [19] Brian Olson, Kevin Molloy, and Amarda Shehu. 2011. In search of the protein native state with a probabilistic sampling approach. *Journal of Bioinformatics and Computational Biology* 9, 03 (2011), 383–398.
- [20] E.F. Pettersen, T.D. Goddard, C.C. Huang, G.S. Couch, D.M. Greenblatt, E.C. Meng, and T.E. Ferrin. 2004. UCSF Chimera—A visualization system for exploratory research and analysis. *J. Comput. Chem.* 25 (October 2004), 1605–1612. Issue 13.
- [21] Amarda Shehu and Erion Plaku. 2016. A survey of computational treatments of biomolecules by robotics-inspired methods modeling equilibrium structure and dynamics. *Journal of Artificial Intelligence Research* 57 (2016), 509–572.
- [22] Guang Song and Nancy M. Amato. 2000. A motion planning approach to folding: from paper craft to protein folding. In *Proc. IEEE Int. Conf. Robot. Autom. (ICRA)*. 948–953.
- [23] Guang Song, Shawna Thomas, Ken A. Dill, J. Martin Scholtz, and Nancy M. Amato. 2003. A path planning-based study of protein folding with a case study of hairpin formation in protein G and L. In *Proc. Pacific Symposium of Biocomputing (PSB)*. 240–251.
- [24] Haixin Sui and Kenneth H. Downing. 2010. Structural basis of interprotofilament interaction and lateral deformation of microtubules. *Structure* 18, 8 (2010), 1022–1031.
- [25] Karel Svoboda, Christoph F. Schmidt, Bruce J. Schnapp, and Steven M. Block. 1993. Direct observation of kinesin stepping by optical trapping interferometry. *Nature* 365, 6448 (1993), 721–727.
- [26] Xinyu Tang, Shawna Thomas, Lydia Tapia, David P. Giedroc, and Nancy M. Amato. 2008. Simulating RNA folding kinetics on approximated energy landscapes. *J. Mol. Biol.* 381 (2008), 1055–1067.
- [27] Lydia Tapia, Xinyu Tang, Shawna Thomas, and Nancy M. Amato. 2007. Kinetics analysis methods for approximate folding landscapes. *Bioinformatics* 23, 13 (2007), i539–i548.
- [28] Ronald D. Vale, Thomas S. Reese, and Michael P. Sheetz. 1985. Identification of a novel force-generating protein, kinesin, involved in microtubule-based motility. *Cell* 42, 1 (1985), 39–50.
- [29] Junmei Wang, Romain M. Wolf, James W. Caldwell, Peter A. Kollman, and David A. Case. 2004. Development and testing of a general amber force field. *Journal of Computational Chemistry* 25, 9 (2004), 1157–1174.
- [30] Ahmet Yildiz, Michio Tomishige, Ronald D. Vale, and Paul R. Selvin. 2004. Kinesin walks hand-over-hand. *Science* 303, 5658 (2004), 676–678.